Article:

eprints@whiterose.ac.uk
https://eprints.whiterose.ac.uk/

3
4
5 **Spray-cast multilayer organometal perovskite solar cells fabricated in air**
6
7 David. K. Mohamad, Jonathon Griffin, Christopher Bracher, Alexander T. Barrows and
8 David G. Lidzey*
9
10 Dr D. K. Mohamad, Dr J. Griffin, Mr C. Bracher, Dr A. T. Barrows and Prof. D. G. Lidzey
11 Department of Physics & Astronomy, University of Sheffield, Hicks Building, Hounsfield
12 Road, Sheffield, S3 7RH, UK
13 E-mail: d.g.lidzey@sheffield.ac.uk
14
17
18 Spray-coating is a versatile coating technique that can be used to deposit functional films over
19 large areas at speed. Here, we use spray-coating to fabricate inverted perovskite solar cell
20 devices in which all of the solution-processible layers (PEDOT:PSS, perovskite and PCBM)
21 are deposited by ultrasonic spray-casting in air. Using such techniques, we fabricate all-spray-
22 cast devices having a champion power conversion efficiency (PCE) of 9.9%. Such
23 performance compares favorably with reference devices spin-cast under a nitrogen
24 atmosphere that have a champion PCE of 12.8%. We ascribe losses in device efficiency to
25 lower surface coverage and reduced uniformity of the spray-cast perovskite layer.
26
27 **1. Introduction**

28 Recent research efforts have driven a remarkable increase in the power conversion efficiency

29 (PCE) of organometal halide perovskite solar cells (PSCs). Such materials combine high

30 charge-carrier mobility, efficient light absorption and can be deposited via low-temperature

31 solution-based processes. Since the early work of Kojima et al.[1], PCEs have risen from 3.8%

32 to 20.1%[2] in state-of-the art devices. As such, PSCs have become an important photovoltaic

33 technology and represent a potentially promising low-cost solution to increasing global

34 demand for sustainable energy.

35

36 At present, the majority of studies that address the fabrication of PSCs are heavily reliant on

37 spin-casting the active layer materials[3]. While spin-casting can be used to create films having

38 well controlled thickness and a high degree of uniformity, it is clearly not compatible with

39 manufacture over large areas or high-volume. To address this issue, a number of studies have

40 already explored the application of scalable deposition techniques for PSC device fabrication,

41 including inkjet printing[4], slot-die coating[5, 6], doctor-blading[7], and spray-casting[8, 9]. Since

42 PSC devices most often comprise a number of different layers that either harvest sunlight or

43 transport charges, a holistic understanding of the necessary multi-layer deposition processes is

44 required. Ultimately, any practical PSC fabrication process must be scalable, however this has

45 only been demonstrated in a few cases. One study of note demonstrated fully doctor-bladed

46 devices utilizing vacuum-processed back contacts having an average PCE of over 10%[5]; a

47 value that reduced to 3.4% when the electrode was instead printed[6]. Previously, we

48 demonstrated that inverted perovskite solar cells can be deposited by ultrasonic spray-

49 coating[8], however the only layer that was deposited by spray-coating was the active

50 perovskite precursor. To address this, we now demonstrate the fabrication of spray-cast

51 perovskite devices in which all layers (the active layer and both PEDOT:PSS and PCBM

52 charge transporting layers) are spray-cast, with deposition performed under ambient

53 conditions. As far as we are aware, this is the first realization of an "all-spray" PSC. In our

54 work, we use a perovskite layer based on the well characterized 3:1 MAI:PbCl$_2$ precursor

55 formulation that is well suited to a planar inverted perovskite solar cell architecture[10], with

56 champion all-spray devices reaching a PCE of 9.9%. Importantly, we achieve deposition

57 speeds over ten times greater than those previously reported by doctor blading methods

58 (which typically have web speeds of 1-20 mm s^{-1} [5, 6]), a result that highlights the commercial

59 relevance of spray-coating for high-volume PSC fabrication.

60

61 **2. Results and discussion**

62 Spray-coating was carried out using a Prism ultrasonic spray-coating system supplied by

63 Ultrasonic Systems, Inc. Here, the oscillation of a piezo-electric tip breaks a solution of

64 interest into a fine mist that is then directed to the surface of interest via a focused nitrogen

65 gas jet – see **Figure 1**(a) and (b). During film spraying, the spray-head is passed over the

66 surface at a fixed height. From extensive optimization trials, we were able to adjust film

67 thickness and drying rates via control of lateral head-speed, solution concentration and

68 substrate temperature. Thin-film deposition typically involves a two-stage process, in which

69 following spray-coating, substrates are transferred to a second hot-plate for extended thermal

70 annealing (with all processes performed in air). Clearly a practical manufacture process would

71 utilize a moving web, with techniques such as infra-red heating to accelerate such annealing

72 steps[11].
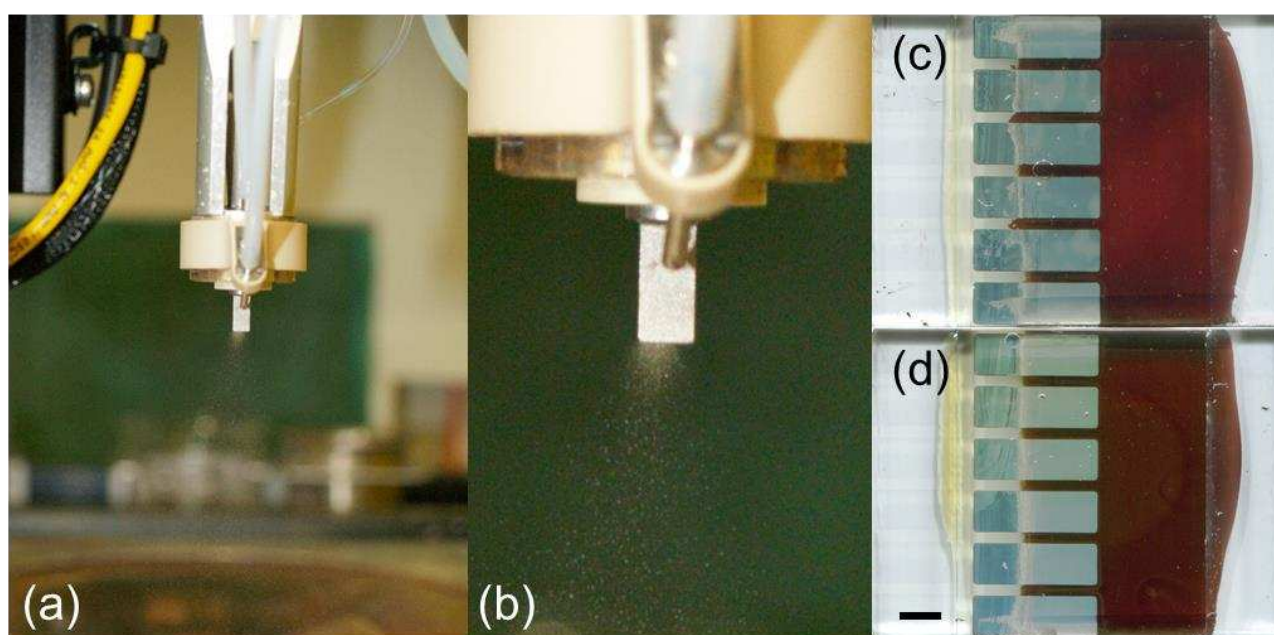
73

74 **Figure 1** – Ultrasonic spray-coating and completed perovskite solar cells: photographs of the

75 spray-coating head under operation (a), close up (b), completed spray-coated (c) and spin-

76 coated (d) perovskite solar cells (2mm scale-bar inset).

77

78 Here, we developed and optimized a series of different spray-coating processes and inks to

79 deposit the PEDOT:PSS hole extraction layer, the $MAI:PbCl_2$ precursor and the PCBM

80 electron-extracting layer. For comparative purposes, the deposition of all layers was explored

81 by both spin-casting and spray-casting. More details are given in Experimental Methods. We

82 tabulate all deposition parameters and ink formulations in Table 1 (see Methods).

83

84 PSC devices were fabricated on pre-patterned glass-ITO substrates. Each substrate consisted

85 of six independent cells having an active area of 4 mm^2, whose size was defined by the

86 overlap of anode and cathode stripes. Note that although six PSC devices are fabricated per

87 substrate, we omit the two edge devices due to defects associated with film formation at the

88 substrate edge.

89

90 Briefly, to spin-cast PEDOT:PSS we have utilized the commercial ink formulation Clevios

91 PVP AI4083 supplied by HC Stark without further modification. For spray-coating, Clevios

92 PVP AI4083 was instead mixed with ethylene glycol (EG) and isopropyl alcohol (IPA) at a

93 ratio 2:8:1 (by volume) of PEDOT:PSS : IPA : EG. Here, the IPA was used to enhance

94 wetting[12] whereas EG improved the film uniformity[13].

95

96 The precursor perovskite films (3:1 MAI:PbCl$_2$ solution in DMF) were coated on the

97 ITO/PEDOT:PSS anode under ambient lab conditions maintained at 20±2ºC and 30±5% RH.

98 It was found that device performance could be significantly enhanced through the addition of

99 1% (by volume) hydrogen iodide (see Figure S1-2). At present the underlying mechanism for

100 this improvement is unclear. However, it has been suggested that efficiency gains may

101 originate from a reduction in PbI$_2$ impurities[14], or from enhanced solubility of solvated

102 perovskite crystals leading to increased surface coverage[15].

103

104 PC$_{70}$BM solutions were prepared by both spin- and spray-casting. Spin-cast films were

105 deposited in a nitrogen-filled glove-box, while spray-cast films were cast in air before being

106 transferred to a vacuum oven and baked for 1 hour at 60 ºC to remove trapped oxygen and

107 moisture. A cathode of LiF and Aluminum was then thermally evaporated after which devices

108 were encapsulated using a UV-treated epoxy before testing. Images of completed

	Device A	Device B	Device C	Device D	Device E
PEDOT	Spin	Spray	Spin	Spray	Spray
Perovskite	Spin	Spin	Spray	Spray	Spray
PCBM	Spin	Spin	Spin	Spin	Spray
PCE (%)	**12.8** (12.1±0.9)	**12.0** (10.7±1.8)	**11.4** (9.8±1.1)	**10.3** (8.6±1.5)	**9.9** (7.1±1.7)
FF (%)	**77** (74±4)	**72** (68±4)	**74** (69±4)	**75** (69±6)	**70** (60±8)
Jsc (mA/cm2)	**18.0** (18.1±0.2)	**18.9** (18.5±0.3)	**17.6** (15.9±1.0)	**16.2** (15.5±0.8)	**16.7** (15.6±0.6)
Voc (V)	**0.93** (0.91±0.02)	**0.91** (0.85±0.09)	**0.92** (0.89±0.03)	**0.86** (0.80±0.07)	**0.87** (0.74±0.11)

109 spray-cast and spin-cast PSC devices are shown in **Figure 1**(c) and (d) respectively.

110 **Table 2** – Performance metrics of perovskite solar cells with spin-cast and spray-cast

111 PEDOT:PSS layers, PCBM and perovskite precursor layers. Champion cell data is shown in

112 bold. Average and standard deviations are displayed in parenthesis.

113

114 Devices were characterized by measuring their J-V curves under 1 Sun AM1.5G simulated

115 solar illumination (see methods). To explore the homogeneity of photocurrent generation, we

116 have also used laser-beam induced imaging (LBIC). Here a laser at 405 nm was focused to a

117 point and raster scanned across the surface with varying step sizes, ranging from 1 µm to 50

118 µm, with the photocurrent recorded using a lock-in amplifier.

119

120 We first discuss the effect of spray-casting the PEDOT:PSS hole extraction layer. This is

121 illustrated in Table 2 and **Figure 2**(a). It can be seen that the all-spin cast device (Device A)

122 has an average PCE of 12.1% compared to an average of 10.7% PCE for a device

123 incorporating a spray-cast PEDOT:PSS film (Device B). This reduction in device efficiency

124 results from a reduced average FF (from 74% to 68%) and reduced V_{OC} (from 0.91V to

125 0.85V) respectively. The reduced FF is clearly seen by inspection of the J-V curves from

126 perovskite solar cells (see Figure 2(a)), most notably near short-circuit where leakage effects

127 are dominant (a larger leakage current is observed in Device B vs Device A)[16]. We attribute

5

128   this effect to the EG rheology modifier added to the PEDOT:PSS ink that facilitates its spray-

129   coating which significantly reduces sheet resistance[17]. We believe that this reduction in sheet

130   resistance leads to a significant increase in parasitic in-plane leakage currents. We tentatively

131   assign the reduced V_{OC} also seen in Device B to increased roughness and poorer perovskite-

132   PEDOT surface coverage[18].

133
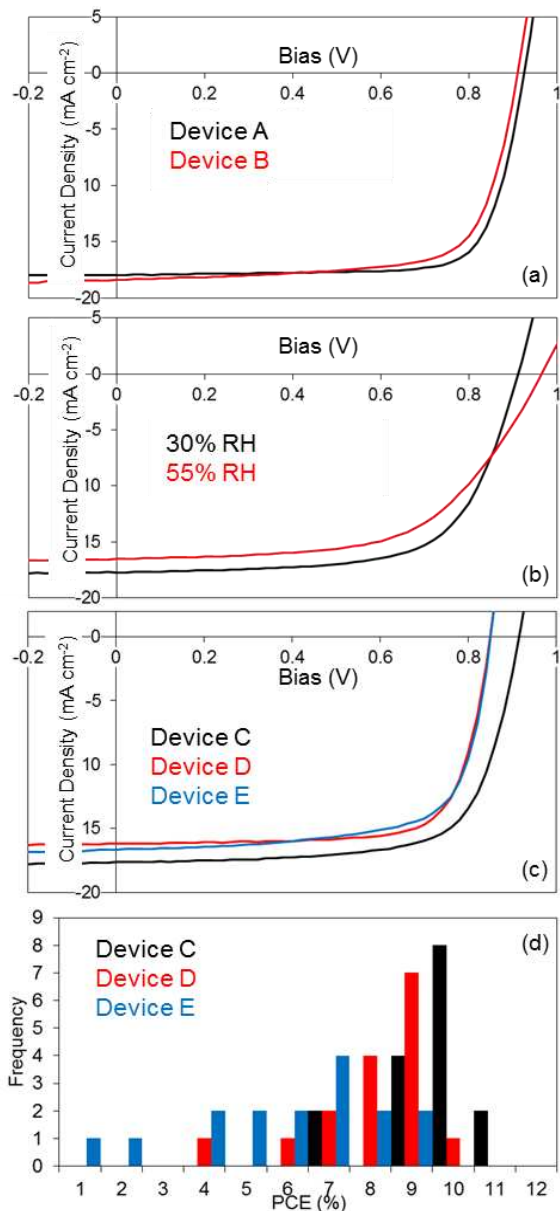
Figure 2 – Development of the all-sprayed perovskite solar cell. J-V traces from champion

cells measured under 1 Sun AM1.5G irradiation whilst sweeping applied bias from +1V to -

1V. Part (a): Device A (black line) and Device B (red line). Part (b): Effect of ambient

humidity on spray-coated device performance. Device C processed at 30% (black line) and

55% humidity (red line). Part (c): Device C (black line), Device D (red line) and Device E

(blue line). Part (d): PCE histogram of perovskite solar cells prepared by different processing

methods: Device C (black bars), Device D (red bars) and Device E (blue bars).

143 Having successfully demonstrated the feasibility of spray-casting PEDOT:PSS thin-films for

144 perovskite solar cells, we now explore the effect of spray-casting both the perovskite

145 precursor and the PCBM. Here, 16 cells were fabricated under each condition (Device C to E),

146 with device performance metrics summarized in Table 2. It can be seen that the spray-cast

147 perovskite process (Device C) creates devices having an average efficiency of 9.8% with

148 standard deviation of 1.1% indicating good control over process repeatability. Champion cells

149 exhibit a PCE of 11.4% – a value that compares well with the range of device efficiencies

150 seen in the all-spin-cast devices (Device A). Such results are in good agreement with our

151 earlier findings in which we demonstrated that devices based on spray-cast perovskite films

152 perform comparably to those in which this layer is deposited by spin-casting[8].

153

154 During our device optimization program, we explored the effect of ambient humidity during

155 processing on the performance of the spray-cast devices. Devices were fabricated that

156 incorporated a spray-cast perovskite layer (Device C) that was deposited in either a low (30%)

157 or a high (55%) relative humidity (RH) environment. Representative J-V traces are shown in

158 Figure 2(b). It can be seen that increased RH appears to reduce average PCE from 10.3% to

159 8.3%; an effect resulting from significant losses in FF and J_{SC} in spite of an increased V_{OC}

160 (see Table S1). We note that previous work has shown that elevated RH has been found to

161 enhance V_{OC} either by "self-healing" of the perovskite lattice[19] or by promoting grain

162 growth[20] in spin-cast PSCs. Despite small gains in V_{OC} however, it appears that a low-

163 humidity environment appears most suitable for depositing high efficiency PSCs by spray-

164 casting. Although the mechanism behind this effect is not presently known, we expect low

165 RH conditions to increase the surface energy of a hydrophilic surface[21]. Therefore ink

166 droplet wetting of the PEDOT substrate surface may be enhanced by low ambient humidity; a

167 process central to the preparation of high efficiency spray-cast devices. For this reason all data

168   presented here (except that in Figure 2(b)) was taken from devices processed in a low

169   humidity environment.

170

171   In Table 2 and Figure 2(c), we compare the performance of 'all-spray' devices incorporating

172   spray-cast PEDOT:PSS, perovskite and PCBM layers (Device E) against devices based on

173   spray-cast perovskite but spin-cast PEDOT:PSS and PCBM (Device C) or with spray cast

174   PEDOT:PSS and spin-cast PCBM (Device D). Here, we note that to optimize device

175   performance, it was necessary to incorporate a slightly thicker PCBM layer (200±5nm) in

176   devices that contained a spray-cast perovskite-precursor layer (Devices C, D and E) compared

177   to those incorporating a spin-cast perovskite-precursor (150±5nm) (Devices A and B). As we

178   demonstrate below, this was necessary as the spray-cast perovskite-precursor film on

179   PEDOT:PSS is characterized by both increased thickness variation and variable surface

180   coverage compared to equivalent spin-cast films. Nevertheless, our results in Table 2 indicate

181   that spray-casting PEDOT:PSS and PCBM layers seem to have little effect on the average J_{SC}

182   of spray-cast perovskite-based devices. It is clear however that spray-casting PEDOT:PSS and

183   PCBM both reduce average device V_{OC} from 0.89 in Device C to 0.80 and 0.74 V in Device

184   D and E respectively. We believe this effect results from reduced surface coverage of the

185   perovskite layer (vide infra). Such reduced surface coverage necessitates the use of a thicker

186   PCBM layer to more completely planarize the underlying perovskite film and optimize device

187   performance. This conclusion is supported by PCBM thickness tuning studies carried out on

188   spin-cast devices (see Figure S3). It is apparent that spray-casting PCBM also contributes to

189   efficiency losses through reduced average FF that is reduced from 69 to 60% in Devices D

190   and E respectively. This effect is attributed to the fact that spray-cast PCBM is processed in

191   air and may well have an increased density of traps[22] and thus lead to higher series resistance.

192   It is clear that reduced uniformity or variable surface-coverage in spray-cast perovskite and

193   PCBM films also leads to a larger spread in device performance combined with a lower

9

194 average value; a result illustrated by the PCE histogram of Devices C to E in Figure 2(d).

195 Complete performance metrics are shown in Figure S4.

196
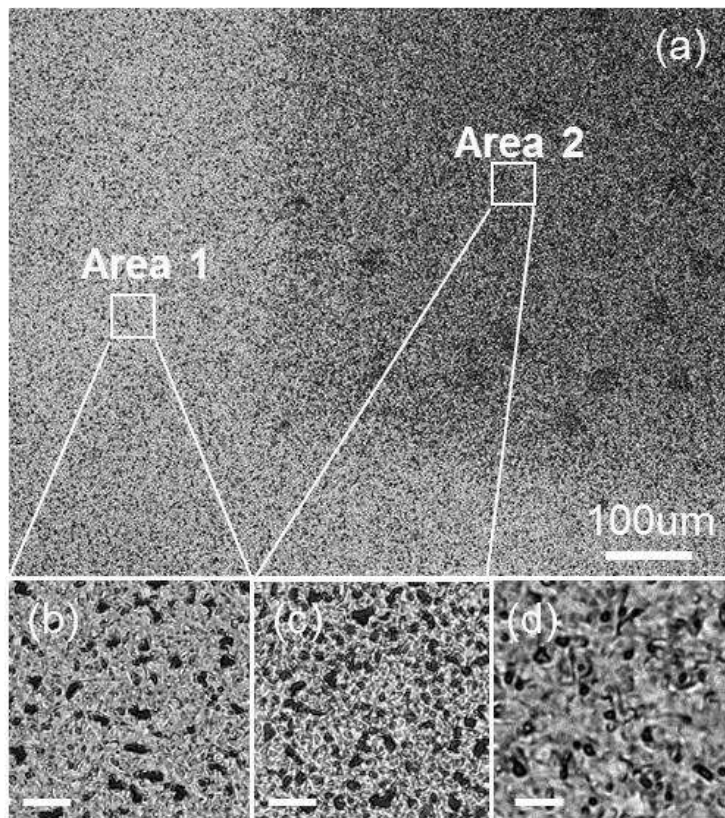
197

198 **Figure 3** – Reflection optical microscope images of spray-coated perovskite films prepared

199 on spin-coated PEDOT:PSS: 10x magnification (a) 100 µm scale bar inset, 50x magnification

200 (b) and (c) of bright (Area 1) and dark (Area 2) regions in image (a) respectively. A

201 comparative 50x magnification image of a spin-coated film is shown in image (d) with 10 µm

202 scale-bar inset.

203

204 The reduced-uniformity of the spray-cast perovskite layer is illustrated in **Figure 3**, where we

205 show optical microscope images (taken in reflection) of a spray-cast perovskite/PEDOT:PSS

206 thin-film at low magnification in part (a). Here, it can be seen that brighter and darker areas

207 are evident which correspond to areas of higher and lower surface coverage as shown in

208 Figure 3(b) and (c) (recorded at higher magnification). From analysis of these images, we

209 determine a surface coverage of the bright and dark regions as 74% and 62% respectively.

210 This compares to analogous spin-cast films that have a surface coverage of 70% (see Figure

211 3(d)). Indeed, by comparing data presented in Table 2 we find that the thicker PCBM films

212 (used in Devices C to E) reduce FF and J_{SC} due to increased series resistance and increased

213 optical-absorption losses respectively (see Figure S3). In all our devices therefore, we find

214 there exists an optimum PCBM thickness defined by the need to adequately planarize the

215 underlying perovskite while minimizing the deleterious effects of reduced light absorption

216 and increased series resistance caused by excessively thick PCBM films. The reduced

217 uniformity of the spray-cast perovskite films (see Figure S5-7) thus necessitate thicker PCBM

218 layer compared to spin-cast analogues, a result that accounts for the reduced efficiency of

219 Device C compared to Device A.
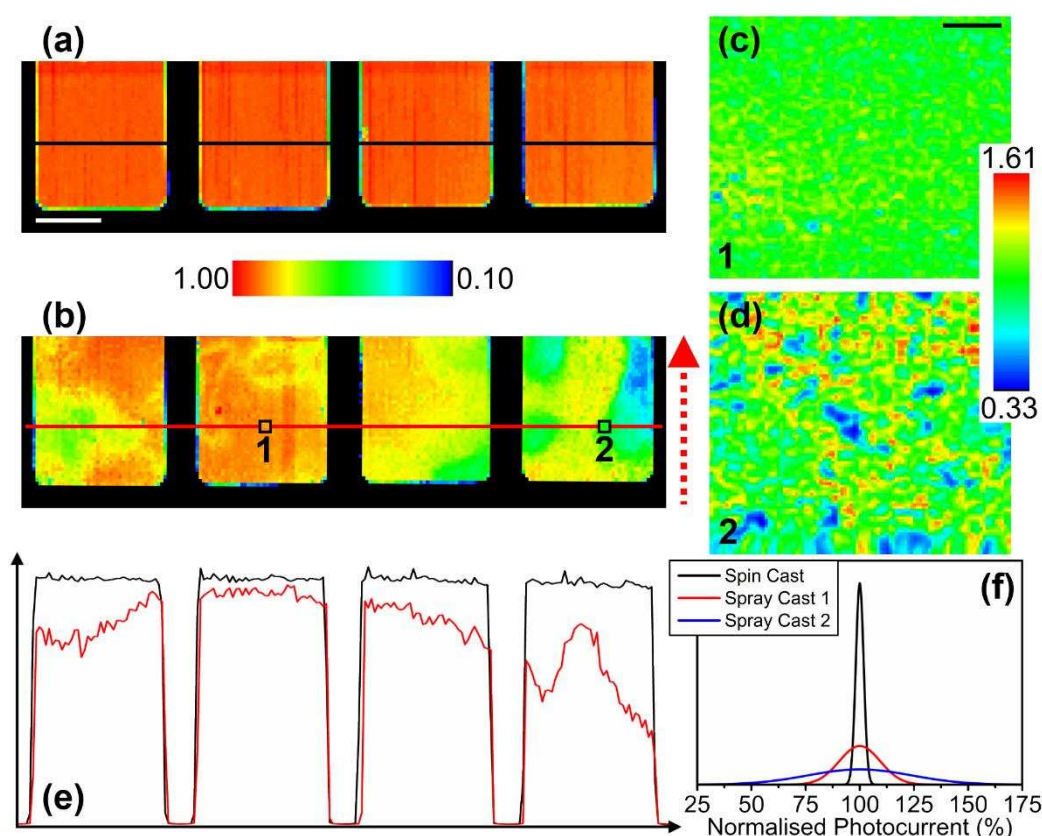
220

221 **Figure 4** – Comparing the uniformity of spin-cast and spray-cast perovskite solar cells by

222 LBIC: low magnification images of Device A (a) and Device C (b) with 1 mm scale-bar inset.

223 Red dashed arrow shows the coating direction. High magnification images of marked areas of

224 Device C are shown in (c) and (d) with 20um scale-bar shown inset. Line profiles from (a)

225 and (b) are shown in (e) and histogram of photocurrent data from images (c), (d) and a spin

226 cast device (not shown) is shown in (f).

227

228 To further characterize the spin-cast and spray-cast films, we have also used LBIC imaging to

229 determine the spatial homogeneity of the photocurrent. This is shown in **Figure 4** where we

230 plot LBIC images across a series of cells from Device A (shown in part (a)) and Device C

231 (part (b)). It is immediately apparent that the photocurrent generated across spin-cast cells are

232 relatively uniform over each cell, while significant variations are observed across the spray-

233 cast cells, with fluctuations in photocurrent of the order of 3.4% and 15% occurring over mm-

234 lengthscales respectively (see part (e)). Higher resolution images recorded from Device C

235 plotted in parts (c) and (d) (corresponding to the regions identified using boxes in part (b)),

236 similarly indicate smaller-scale fluctuations in photocurrent occurring over µm-lengthscales.

237 We also illustrate the differences in the LBIC images in Figure 4(e) and (f), where we plot a

238 horizontal section through the LBIC images recorded from Device A (black line) and Device

239 C (red-line). A histogram illustrating the spread in photocurrent recorded across Device A and

240 the two highlighted regions in device C (Figure 4(f)) similarly highlight the greater spread in

241 photocurrent recorded from the spray-cast devices.

242

243 We speculate that the large-scale fluctuations observed in spray-cast films (see Figure 4(b))

244 most likely result from interactions between the gas-jet and precursor wet-film. Given the

245 rapid drying-rate required to form optimal microstructure, there is insufficient time (10-15s)

246 to allow the wet-film to level. Therefore, these macroscopic thickness fluctuations are

247 effectively "frozen" into the final dry-film and are then reflected in variations in surface

248 coverage in the final perovskite film that occur at µm-length scales. We are confident that by

249 using improved spray-jet homogenization schemes it will be possible to improve coating

250 quality. We also anticipate that the techniques and material system we have used here will be

251 readily scalable to larger-size device areas; indeed we have previously used ultra-sonic spray

252 coating to fabricate arrays of organic photovoltaic devices over an area of 25 cm^{2}[23] and

253 individual devices having an active area of 1.6 cm^{2}[13]. Finally, we note that the DMF solvent

254 used here is very toxic, and that any manufacture process must consider both the safety of the

255 process operators together with the effects on the environment. We note that polymer

256 photovoltaic devices can be fabricated by replacing the frequently-used halogenated solvents

257 with non-halogenated solvent blends that are less environmentally hazardous[24]. We expect

258 similar progress to be made in the development of processes suitable for spray-casting

259 perovskite photovoltaics. Indeed, we note that recent work using a mixture of γ-butyrolactone

260 together with an alcohol and an acid has been used to create pin-hole free films by both spin-

261 coating and blade-coating which were then used to create efficient PV devices[25].

262

263 **3. Conclusions**

264 We have successfully demonstrated the applicability of spray-coating as a scalable technique

265 to prepare PSC devices by depositing all solution-processed layers with this technique.

266 Overall, our all-spray coated PSCs have an average PCE of 7.1% and a remarkable peak

267 efficiency of 9.9%; a value that is reduced relative to devices in which all layers are fabricated

268 by spin-coating (12.8% peak, 12.1% average) as a result of reduced uniformity and lower

269 surface coverage of the perovskite layer. Despite this reduction in efficiency, we note that the

270 speed at which the surface is coated (220 mm s^{-1}) represents the fastest lateral velocity at

271 which perovskite precursor films have so-far been deposited. Our work therefore represents a

272 significant step towards the realization of a truly scalable PSC manufacture process.

273

274 **Notes and References**

275 [1] A. Kojima, K. Teshima, Y. Shirai, T. Miyasaka, Journal of the American Chemical
276 Society 2009, **131**, 6050.
277 [2] W. S. Yang, J. H. Noh, N. J. Jeon, Y. C. Kim, S. Ryu, J. Seo, S. I. Seok, Science 2015,
278 **348**, 1234.
279 [3] J. F. Yan, B. R. Saunders, Rsc Advances 2014, **4**, 43286.
280 [4] S.-G. Li, K.-J. Jiang, M.-J. Su, X.-P. Cui, J.-H. Huang, Q.-Q. Zhang, X.-Q. Zhou, L.-
281 M. Yang, Y.-L. Song, Journal of Materials Chemistry A 2015, **3**, 9092.
282 [5] K. Hwang, Y.-S. Jung, Y.-J. Heo, F. H. Scholes, S. E. Watkins, J. Subbiah, D. J.
283 Jones, D.-Y. Kim, D. Vak, Advanced Materials 2015, **27**, 1241.
284 [6] T. M. Schmidt, T. T. Larsen-Olsen, J. E. Carle, D. Angmo, F. C. Krebs, Advanced
285 Energy Materials 2015, **5**, 1500569.
286 [7] Y. Deng, E. Peng, Y. Shao, Z. Xiao, Q. Dong, J. Huang, Energy & Environmental
287 Science 2015, **8**, 1544.
288 [8] A. T. Barrows, A. J. Pearson, C. K. Kwak, A. D. F. Dunbar, A. R. Buckley, D. G.
289 Lidzey, Energy & Environmental Science 2014, **7**, 2944.
290 [9] J. G. Tait, S. Manghooli, W. Qiu, L. Rakocevic, L. Kootstra, M. Jaysankar, C. A. M.
291 de la Huerta, U. W. Paetzold, R. Gehlhaar, D. Cheyns, P. Heremans, J. Poortmans, Journal of
292 Materials Chemistry A 2016, **4**, 3792; S. Das, B. Yang, G. Gu, P. C. Joshi, I. N. Ivanov, C. M.
293 Rouleau, T. Aytug, D. B. Geohegan, K. Xiao, Acs Photonics 2015, **2**, 680; Z. Liang, S.
294 Zhang, X. Xu, N. Wang, J. Wang, X. Wang, Z. Bi, G. Xu, N. Yuan, J. Ding, Rsc Advances
295 2015, **5**, 60562.
296 [10] P. Docampo, J. M. Ball, M. Darwich, G. E. Eperon, H. J. Snaith, Nature
297 Communications 2013, **4**; H. P. Zhou, Q. Chen, G. Li, S. Luo, T. B. Song, H. S. Duan, Z. R.
298 Hong, J. B. You, Y. S. Liu, Y. Yang, Science 2014, **345**, 542.
299 [11] J. Troughton, C. Charbonneau, M. J. Carnie, M. L. Davies, D. A. Worsley, T. M.
300 Watson, Journal of Materials Chemistry A 2015, **3**, 9123; J. Troughton, M. J. Carnie, M. L.
301 Davies, C. Charbonneau, E. H. Jewell, D. A. Worsley, T. M. Watson, Journal of Materials
302 Chemistry A 2016, **4**, 3471.
303 [12] C. Girotto, D. Moia, B. P. Rand, P. Heremans, Advanced Functional Materials 2011,
304 **21**, 64.
305 [13] N. W. Scarratt, J. Griffin, T. Wang, Y. Zhang, H. Yi, A. Iraqi, D. G. Lidzey, Apl
306 Materials 2015, **3**, 7.
307 [14] J. H. Heo, D. H. Song, H. J. Han, S. Y. Kim, J. H. Kim, D. Kim, H. W. Shin, T. K.
308 Ahn, C. Wolf, T.-W. Lee, S. H. Im, Advanced Materials 2015, **27**, 3424.
309 [15] J. H. Heo, D. H. Song, S. H. Im, Advanced Materials 2014, **26**, 8179.
310 [16] J. Nelson, The Physics of Solar Cells, Imperial College Press, 2003.
311 [17] S. Ashizawa, R. Horikawa, H. Okuzaki, Synthetic Metals 2005, **153**, 5; B. Y. Ouyang,
312 C. W. Chi, F. C. Chen, Q. F. Xi, Y. Yang, Advanced Functional Materials 2005, **15**, 203.
313 [18] G. E. Eperon, V. M. Burlakov, P. Docampo, A. Goriely, H. J. Snaith, Advanced
314 Functional Materials 2014, **24**, 151.
315 [19] G. E. Eperon, S. N. Habisreutinger, T. Leijtens, B. J. Bruijnaers, J. J. van Franeker, D.
316 W. dequilettes, S. Pathak, R. J. Sutton, G. Grancini, D. S. Ginger, R. A. J. Janssen, A.
317 Petrozza, H. J. Snaith, Acs Nano 2015, **9**, 9380.
318 [20] J. You, Y. Yang, Z. Hong, T.-B. Song, L. Meng, Y. Liu, C. Jiang, H. Zhou, W.-H.
319 Chang, G. Li, Applied Physics Letters 2014, **105**.
320 [21] J. W. Whalen, K. Y. Lai, Journal of Colloid and Interface Science 1977, **59**, 483; A.
321 M. Lyakhovich, A. A. Shakov, N. V. Lyalina, Protection of Metals and Physical Chemistry of
322 Surfaces 2010, **46**, 534.
323 [22] C.-Y. Nam, D. Su, C. T. Black, Advanced Functional Materials 2009, **19**, 3552.
324 [23] Y. Zhang, J. Griffin, N. W. Scarratt, T. Wang, D. G. Lidzey, Progress in
325 Photovoltaics: Research and Applications 2016, **24**, 275.

14

326 [24]   J. Griffin, A. J. Pearson, N. W. Scarratt, T. Wang, A. D. F. Dunbar, H. Yi, A. Iraqi, A.
327 R. Buckley, D. G. Lidzey, Organic Electronics 2015, **21**, 216.
328 [25]   K. L. Gardner, J. G. Tait, T. Merckx, W. Qiu, U. W. Paetzold, L. Kootstra, M.
329 Jaysankar, R. Gehlhaar, D. Cheyns, P. Heremans, J. Poortmans, Advanced Energy Materials
330 2016, n/a.

4. Methods

ITO substrates ($20\ \Omega\ \square^{-1}$) purchased from Ossila Limited were first cleaned by sonication in

Helmanex solution, deionized water then isopropyl alcohol (IPA), then dried with compressed

nitrogen and ozone-plasma treated before use. To deposit PEDOT:PSS by spin-coating,

Clevios PVP AI4083 was first filtered through a 0.45 µm PVDF syringe filter and then spin-

cast at 5000 rpm to form a 35±2 nm thick layer that was then annealed in air at 120 °C for 10

minutes prior to use.

For spray-coating, the ultra-sonic tip was held at 40 mm above the substrate surface and

vibrated at 35 kHz while fluid from a coating reservoir above was fed to the tip. The ink

droplets created were directed to the surface using a carrier gas whose pressure was set to 10

psi giving a wide spray pattern (ca 50mm). At the same time, the spray head was robotically

scanned a distance of 150mm over ITO device substrates in a single pass. We also found that

multiple pass spray-routines create poor quality films as they tend to re-dissolve the

underlying films. Unlike airbrush techniques in which droplets contain very little solvent

when they reach the surface, ultrasonic spray-cast films consist of droplets that coalesce to

form a fully wet film before drying[12]. Note that the width of the spray-pattern is significantly

larger than that of the individual device pixels (each having a size (2 x 2) mm^2), and thus

significant heterogeneity across the spray-mist pattern at the sample surface is not anticipated.

Between coating processes, pure solvent was flushed through the ink delivery system before

the next ink reservoir was refilled. Substrates were mounted on a hotplate to ensure stable

elevated temperatures in order to control the wet film drying rate.

23

24 PEDOT:PSS was spray-cast from a Clevios PVP AI4083 PEDOT:PSS:IPA:ethylene glycol

25 (EG) mixture onto substrates held at 40 ℃ (head speed of 40 mm s^{-1}), forming a 70±5 nm

26 thick layer when dry. After 1 min, each substrate was transferred to a second hotplate held at

27 150 ℃ for a further minute to remove the EG. The films were then annealed in air at 120 ℃

28 for 10 minutes prior to use. Lab humidity was controlled with an air conditioning system and

29 a desiccant dehumidifier (Humidity control systems Ltd DC31 T16).

30

Parameter	PEDOT		Perovskite		PCBM	
	spin	spray	spin	spray	spin	spray
Atmosphere	Air	Air	Air	Air	N2	Air
substrate temperature*	ambient	1min @ 40 ℃ / 1min @ 150 ℃	90 ℃	70 ℃	ambient	ambient
annealing	10min @ 120 ℃	10min @ 120 ℃	90 min @ 90 ℃	90min @ 90 ℃	10min @ 80 ℃	1hr vac bake @60 ℃
speed	5000 rpm / 30 s	40 mm s^{-1}	4000 rpm / 30 s	220 mm s^{-1}	1000 rpm / 30 s	169 mm s^{-1}
ink conc	n/a	n/a	500 mg ml^{-1}	200 mg ml^{-1}	50 - 70 mg ml^{-1}	20 mg ml^{-1}
solvent	water	2:8:1 PEDOT:IPA:EG	DMF	DMF	CB	1:1 CF:CB
ink temp.	ambient	ambient	70 ℃	ambient	Ambient	ambient

31 **Table 1** – Summary of thin-film deposition protocols (*) refers to substrate temperature

32 during ink deposition.

33

34 Perovskite precursor solutions were prepared from methyl ammonium iodide (MAI, supplied

35 by Ossila Ltd), hydrogen iodide (Sigma 210021) and $PbCl_2$ (Sigma 203572) and were used as

36 received. Spin-coated samples were cast at a spin-speed of 4000 rpm from a 500 mg ml^{-1} 3:1

37 MAI:$PbCl_2$ solution containing 1% HI in DMF (Sigma 227056). Prior to film deposition, both

38 the substrate and casting solution were held at a temperature of 90 ℃ and 70 ℃ respectively

39 to enable rapid drying of the films and to optimize device performance. Spray-cast perovskite

40 precursor films were deposited from a 200 mg ml^{-1} 3:1 MAI:$PbCl_2$ solution in DMF

41 containing 1% HI (solution at ambient temperature) onto substrates held at 70 ℃ with a head-

42 speed of 220 mm s^{-1}. In all cases, film thickness was determined from post-annealed films at

43 five locations using profilometry. Spray-coated and spin-coated film thickness was adjusted to

44 be within 10% of each other (366 ± 19 nm and 390 ± 22 nm respectively).

45

46 The perovskite films were coated with a PC$_{70}$BM electron-extraction layer (95% purity

47 supplied by Ossila Ltd). Spin-cast films were deposited in a nitrogen-filled glove-box. PCBM

48 solutions for spin-casting were prepared at 50 mg ml^{-1} or 70 mg ml^{-1} in chlorobenzene,

49 creating 150 and 200 nm thick films respectively. For spray-casting, PC$_{70}$BM was dissolved at

50 20 mg ml^{-1} in a 1:1 chlorobenzene : chloroform (by volume) solution. Prior to deposition,

51 solutions were heated to 70 ℃ for 1 hour and then filtered through a 0.45 µm PTFE syringe

52 filter. Spray-coated films were deposited in air at a substrate temperature of 20 ℃ and a head-

53 speed of 169 mm s^{-1} before being transferred to a vacuum oven and baked for 1 hour at 60 ℃

54 to remove trapped oxygen and moisture.

55

56 A cathode of LiF and Aluminum was thermally evaporated at 2 nm at 0.1 Å s^{-1} and 100 nm at

57 1 Å s^{-1} respectively within a vacuum chamber held at ca 10^{-6} mbar. Devices were

58 encapsulated using a UV-treated epoxy (supplied by Ossila Ltd) before testing.

59

60 Solar cell characterization

61 Device performance was tested under ambient conditions using a Newport 92251A-1000 solar

62 simulator (AM1.5). An NREL certified silicon reference cell was used to calibrate the

63 integrated light-output from the simulator to 100 mW cm^{-2} at 25 ℃. Here, an aperture mask

64 (0.025 cm^2) was placed over each solar cell to accurately define the device area and minimize

65 absorption of stray light. PCEs were determined for a cell initially held at +1 V, swept to -1 V

66 and back to +1V a rate of 0.4 V s^{-1}. Performance metrics are quoted from the portion of J-V

67 sweep as the bias is swept from +1 to -1V.

68

69 Laser beam induced current imaging

70 Laser beam induced current (LBIC) maps were performed using a custom-built setup.

71 Mechanically chopped excitation from a 3mW 405 nm diode laser was passed through a

72 spatial filter before being focused to a power density of 27 W cm^{-2}. The sample was mounted

73 on a computer-controlled XY-stage and moved in a sawtooth pattern. For high-resolution

74 images, the beam was focused via a 50X Mitutoyo infinity-corrected objective lens giving a

75 spot size of 1 μm and the stage was moved in 1 μm steps. For low-resolution imaging, the

76 beam was focused via a 10X objective lens giving a spot size of ca 10 μm and the stage was

77 moved in 50 μm steps. The PSC photocurrent was collected with a Stanford Research

78 Systems SR830 lock-in amplifier referenced to the chopped laser. Current generation in PSCs

79 was found to scale linearly with laser power up to, and including, the range of interest.

80
81 **Supporting Information**
82 Supporting Information is available from the Wiley Online Library.
83

94 **The table of contents entry should be 50–60 words long**, and the first phrase should be bold.
95 The entry should be written in the present tense and impersonal style. The text should be
96 different from the abstract text.

97 **Spray-coating is a versatile coating technique that can be used to deposit functional**
98 **films over large areas at speed**. Here, the authors fabricate inverted perovskite solar cell
99 devices in which all of the solution-processible layers are deposited by ultrasonic spray-
100 casting in air leading to all-spray-cast devices having a champion power conversion efficiency
101 of 9.9%.

102

103 **Keyword:** Photovoltaic Devices, Conducting Polymers, Thin films, Solar Cells, Functional
104 Coatings

105

106 David. K. Mohamad, Jonathon Griffin, Christopher Bracher, Alexander T. Barrows and David
107 G. Lidzey*

108

109 **Spray-cast multilayer organometal perovskite solar cells fabricated in air**
110
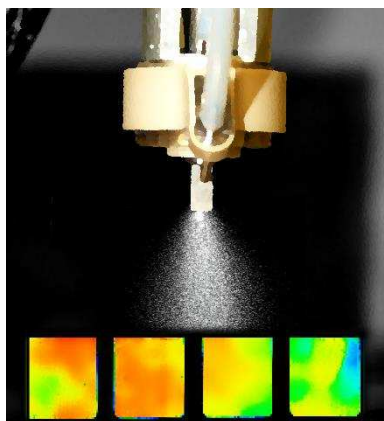
111
112 ToC figure ((Please choose one size: 55 mm broad × 50 mm high **or** 110 mm broad × 20 mm
113 high. Please do not use any other dimensions))
114
115

116   ((Supporting Information can be included here using this template))
117
118   Copyright WILEY-VCH Verlag GmbH & Co. KGaA, 69469 Weinheim, Germany, 2013.

119
120   # Supporting Information
121
122
123   **Spray-cast multilayer organometal perovskite solar cells fabricated in air**
124

125   Author(s), and Corresponding Author(s)* David. K. Mohamad, Jonathon Griffin, Christopher
126   Bracher, Alexander T. Barrows and David G. Lidzey*
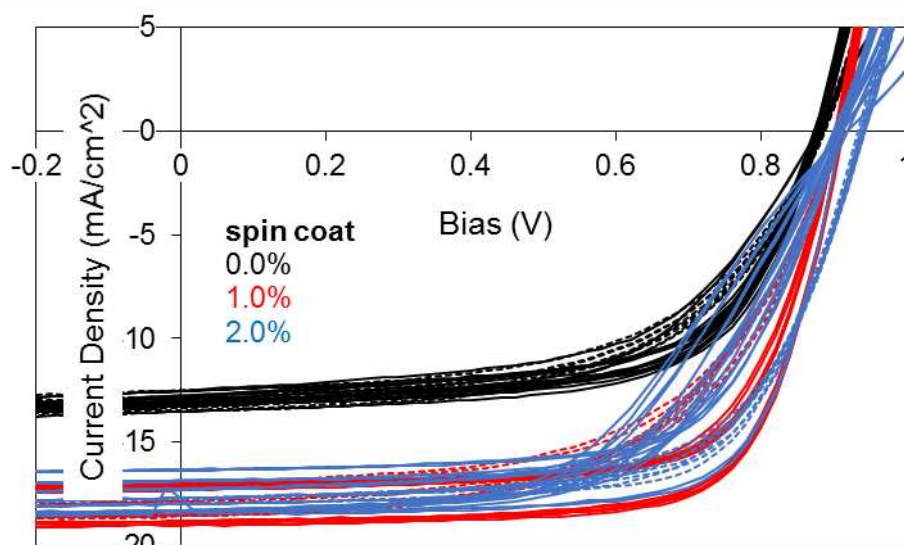
127
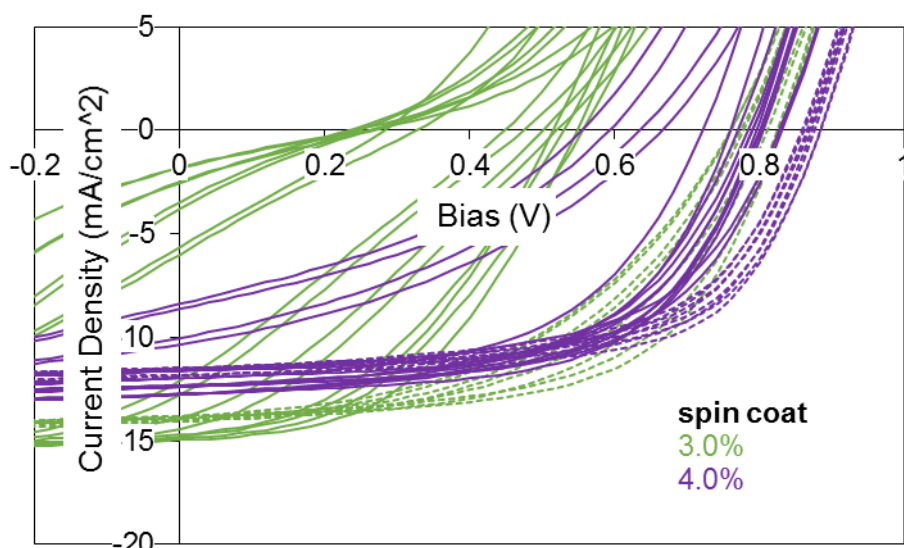
128
129   **Figure S1** - The effect of HI concentration in spin-coated PSCs. PEDOT:PSS and PCBM
130   layers are spin-coated. Solar cell J-V traces measured under 1Sun AM1.5G irradiation whilst
131   cycling applied bias from -1V to +1V and back again.
132

133
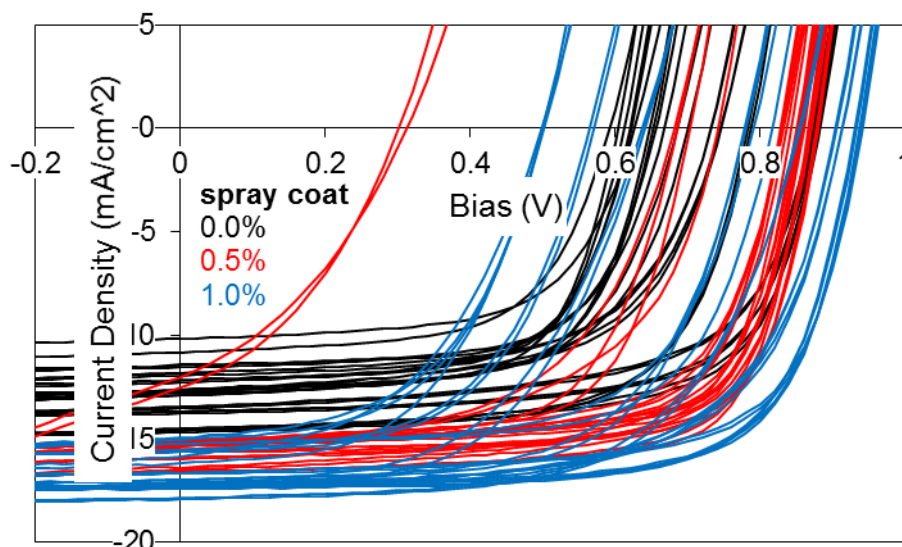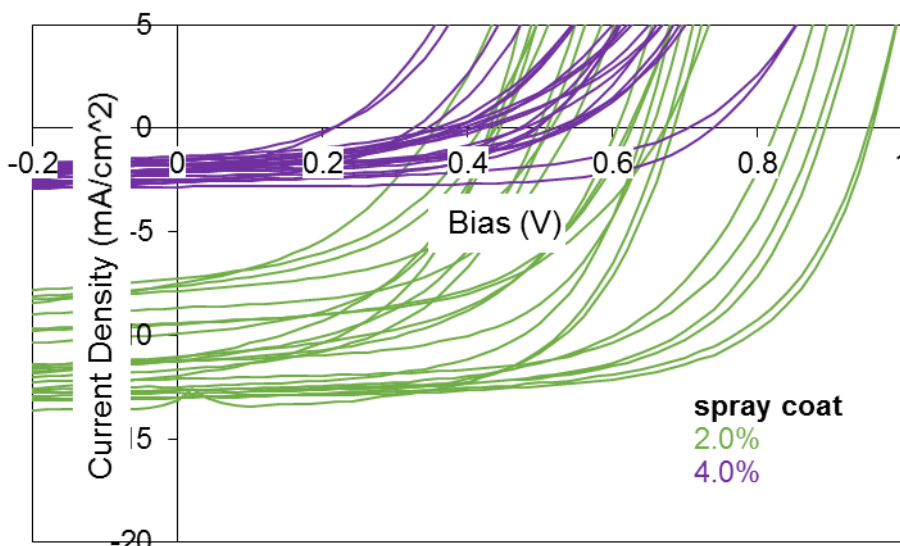
134
135 **Figure S2** - The effect of HI concentration in spray-coated PSCs. PEDOT:PSS and PCBM
136 layers are spin-coated. Solar cell J-V traces measured under 1Sun AM1.5G irradiation whilst
137 cycling applied bias from -1V to +1V and back again.
138

Condition	Low Humidity (30%)	High Humidity (55%)
PCE (%)	**10.7** (10.3±0.5)	**8.2** (9.2±0.7)
FF (%)	**67** (66±2)	**60** (59±5)
J_{sc} (mA/cm^2)	**17.3** (16.8±0.8)	**16.0** (15.3±0.8)
V_{oc} (V)	**0.93** (0.93±0.01)	**0.96** (0.92±0.04)

139 **Table S1** – Performance metrics of perovskite solar cells (Device C) prepared at low and
140 high-humidity. Perovskite precursor has been prepared by spray-casting but PCBM and
141 PEDOT:PSS and PCBM layers have been spin-cast. Champion cell data is shown in bold.
142 Average and standard deviations are displayed in parenthesis
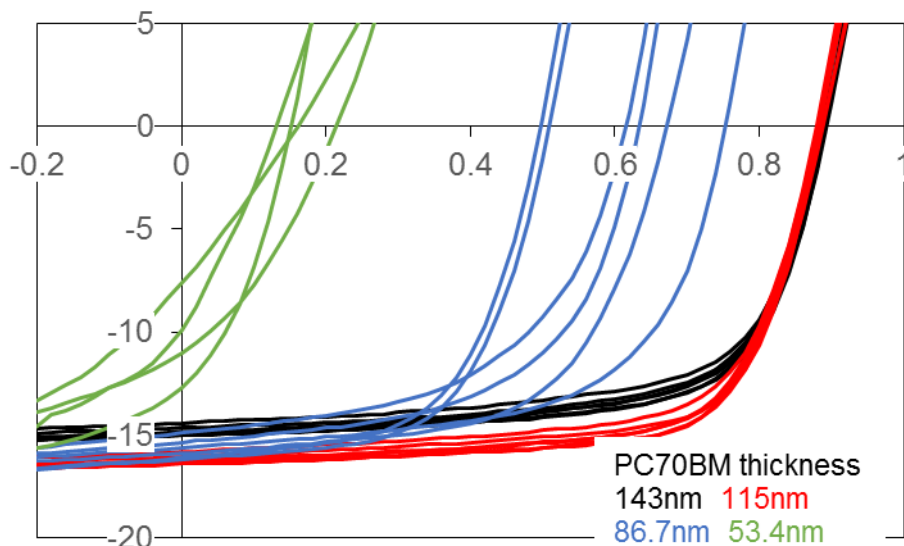
Figure S3 – The effect of spin-coated PCBM thickness in all-spin cast PSCs. Solar cell J-V traces measured under 1Sun AM1.5G irradiation whilst cycling applied bias from -1V to +1V and back again.
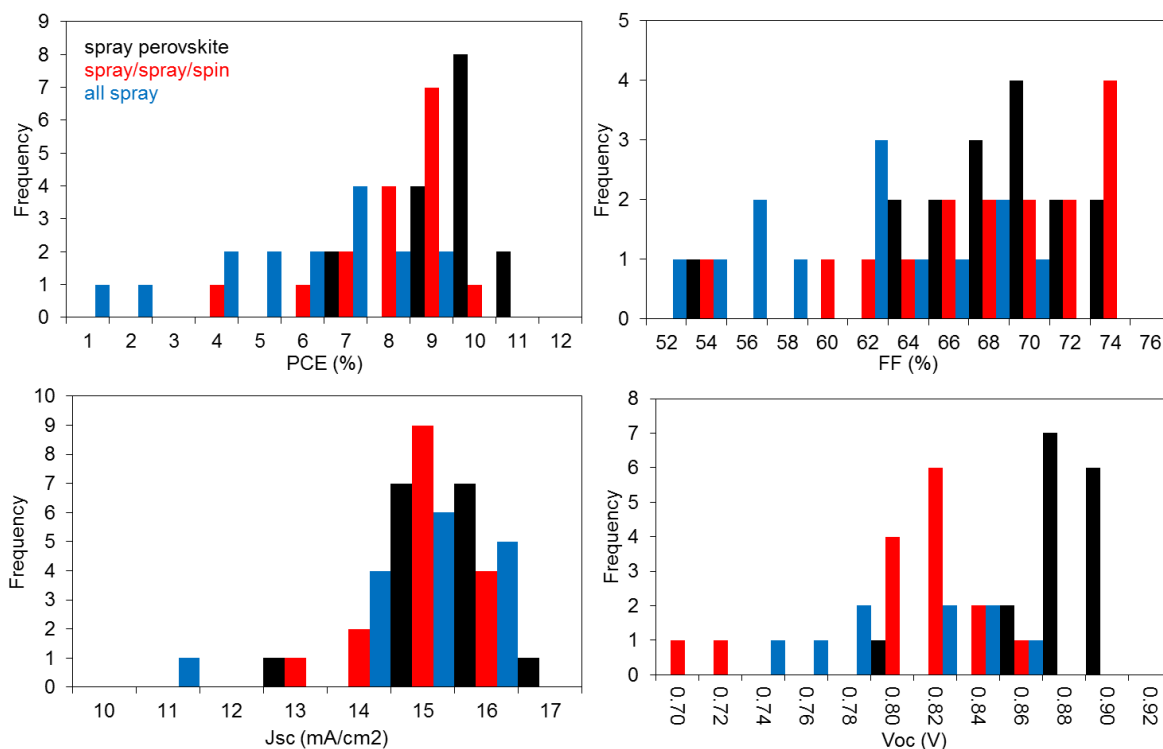
Figure S4 – Histograms of performance metrics from Devices C to E measured from +1 to -1V J-V sweeps under 1 Sun simulated AM1.5G irradiation.

PEDOT: spin-coated
Perovskite: spray-coated
PCBM
120nm spin glovebox
200nm spin glovebox
200nm spin air vac bake
(60C 1hr)
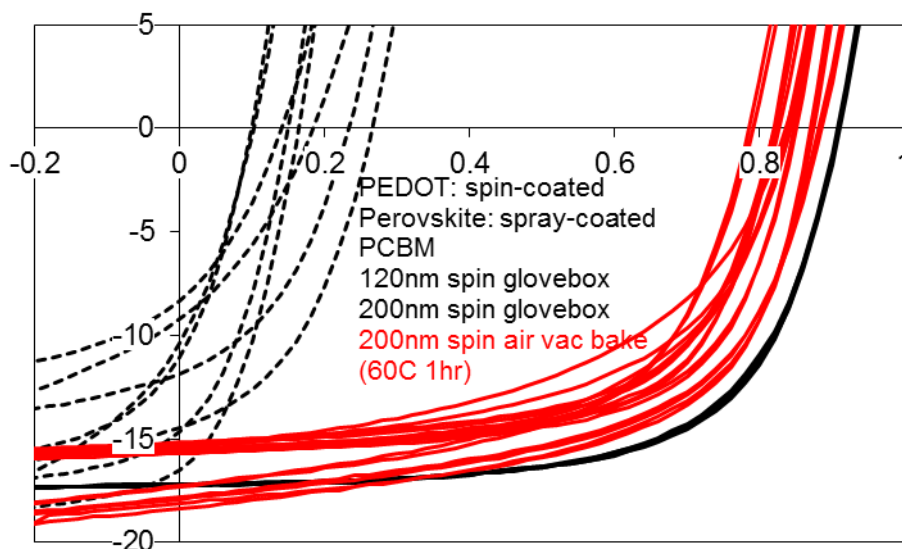
Figure S5 – The effect of spin-coated PCBM thickness in PSCs containing spray-cast MAPbI$_{3-x}$Cl$_x$. PEDOT:PSS layers are spin-coated. Solar cell J-V traces measured under 1Sun AM1.5G irradiation whilst cycling applied bias from -1V to +1V.
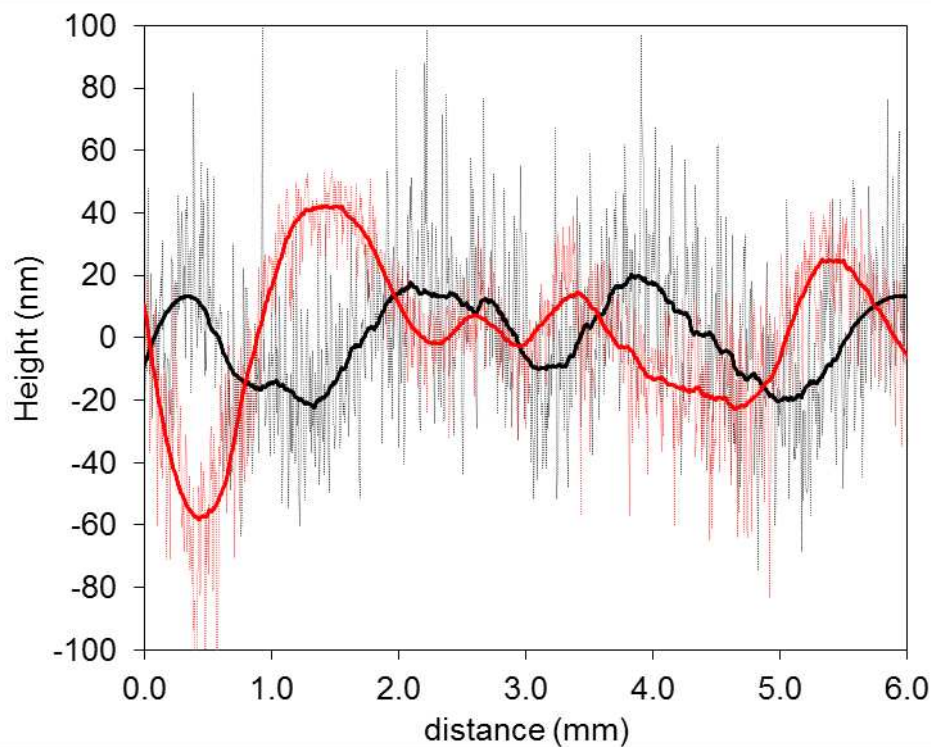
Figure S6 – Surface profiles of spin-coated Device A (black lines) and spray-coated Device C (red lines). Raw data is plotted with thin dotted-lines and filtered data with thick solid-lines.

159

160
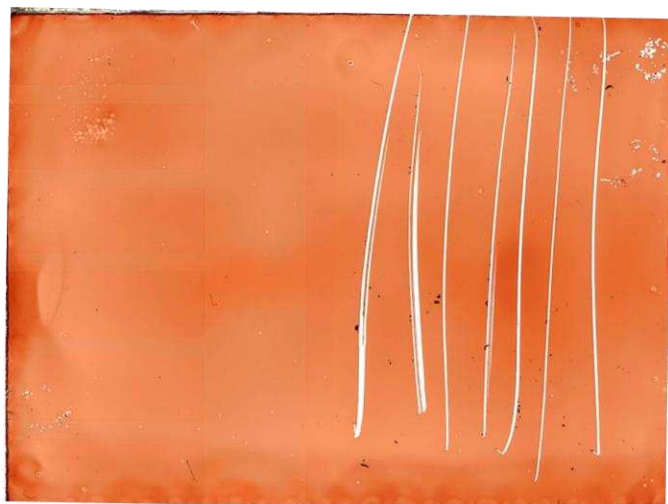
161
162 **Figure S7** – (from top to bottom) Transmission images of PEDOT:PSS(spin)/MAPbI$_{3-}$
163 $_x$Cl$_x$(spin), PEDOT:PSS(spin)/MAPbI$_{3-x}$Cl$_x$(spray) and spray-cast PCBM of ITO glass
164 recorded with a flatbed scanner (Substrates have dimensions of 20x15mm).
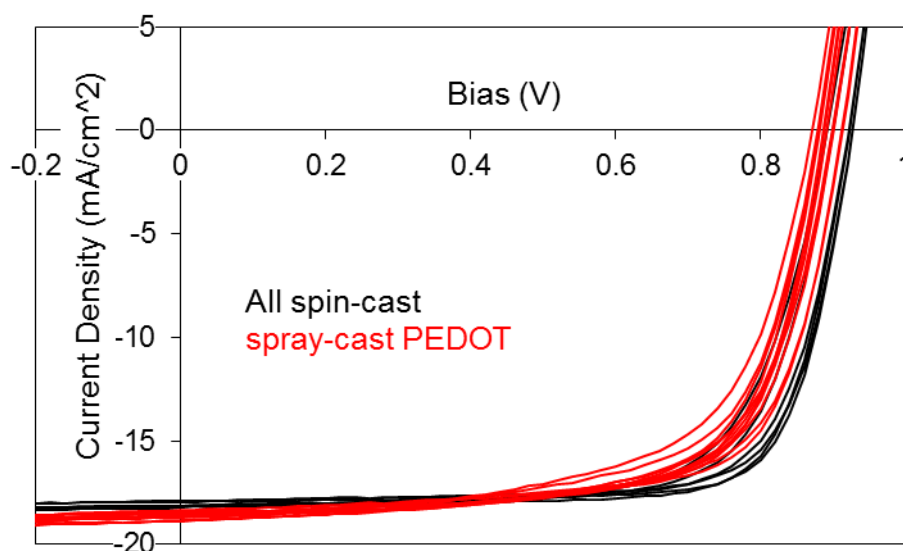
Figure S8 - Demonstration of spray-coated PEDOT:PSS. Solar cell J-V traces measured under 1 Sun AM1.5G irradiation whilst cycling applied bias from -1V to +1V and back again. Device A (black lines) and Device B (red lines). Perovskite precursor and PC70BM layers have been spin-coated.
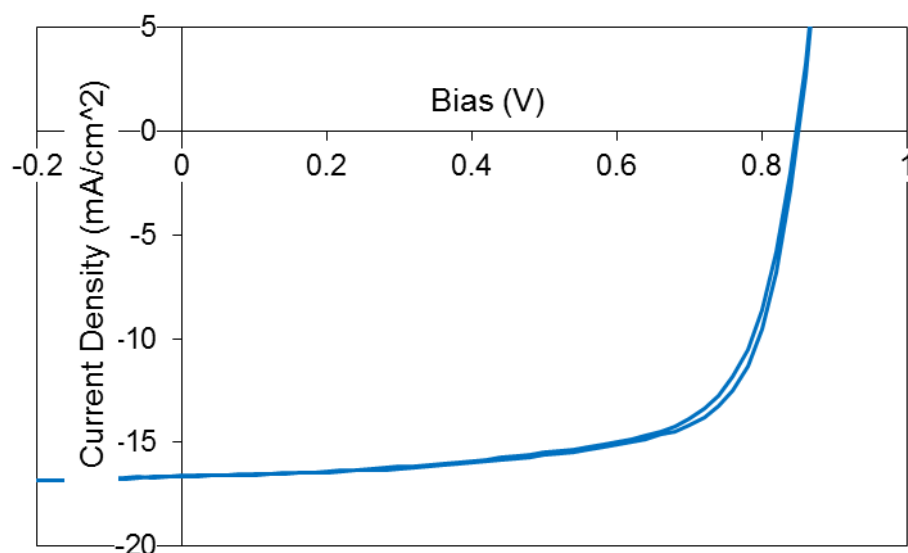
Figure S9 – The effect of hysteresis on the all-sprayed. Solar cell J-V traces measured under 1Sun AM1.5G irradiation whilst cycling applied bias from -1V to +1V and back again (0.4 Vs^{-1})
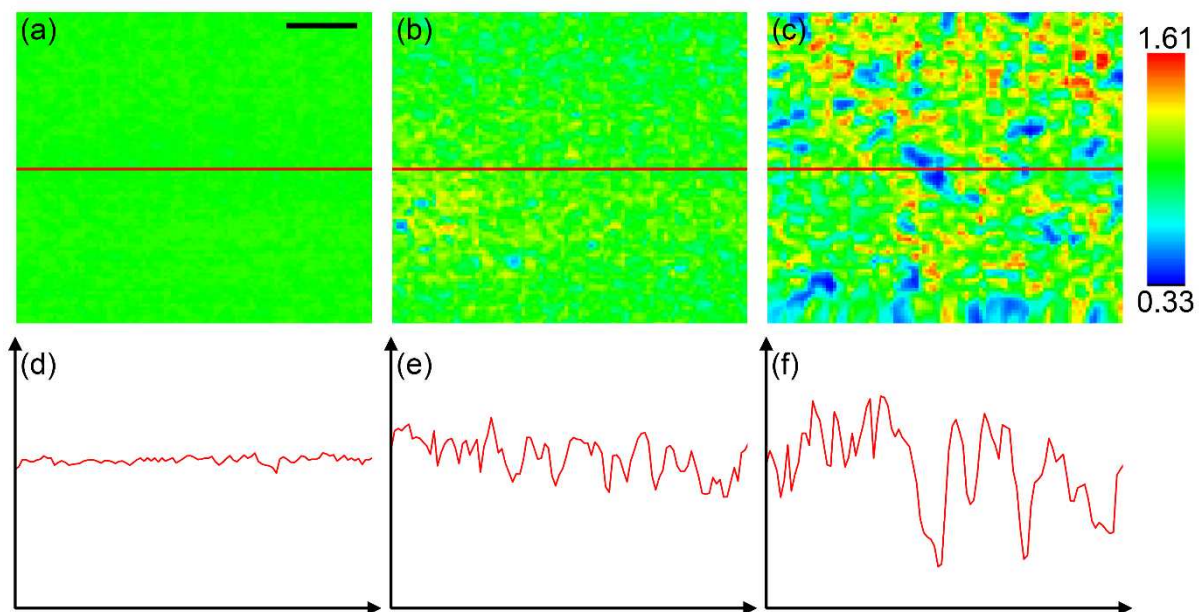
Figure S10 – LBIC images with corresponding horizontal sections from spin-cast Device A (a & d), spray-cast Device C Area 1 (b & e) and Area 2 (c & f). 20um scale bar inset. Section and image data are plotted on matching scales.